 doi:10.20944/preprints202209.0090.v1

Article

Global Dynamics of SARS-CoV-2 Infection with Antibody Response and the Impact of Impulsive Drug Therapy

Amar Nath Chatterjee[1], Dibyendu Biswas[2], Fahad Al Basir[3,*]

[1] Department of Mathematics, K.L.S. College, Nawada, Magadh University, Bodhgaya, Bihar-805110, India
[2] Department of Mathematics, City College of Commerce and Business Administration, 13, Surya Sen Street, Kolkata - 700012, West Bengal, India
[3] Department of Mathematics, Asansol Girls' College, West Bengal-713304, India
* Correspondence: fahadbasir@gmail.com (F. A. Basir)
‡ All authors contributed equally to this work.

Abstract: Mathematical modeling is crucial in investigating the pandemic of the ongoing coronavirus disease (COVID-19). The primary target area of the SARS-CoV-2 virus is epithelial cells in the human lower repertory track. During this viral infection, infected cells can initiate innate and adaptive immune responses to viral infection. Immune response in COVID -19 infection can lead to longer recovery time and more severe secondary complications. We formulate a target cell limited mathematical model by incorporating a saturation term for SARS-CoV-2 infected epithelial cell loss reliant on infected cell levels. Transcritical bifurcation between disease-free and endemic equilibrium points has been analyzed. Global stability of both disease-free and endemic equilibrium is provided. We have seen that the disease-free equilibrium is globally stable for $R_0 < 1$, and endemic equilibrium exists and is globally stable for $R_0 > 1$. Impulsive application of drug dosing has been applied for the treatment of COVID-19 patients. Also, the dynamics of the impulsive system are discussed when a patient takes drug holidays. The numerical simulations are performed in support of our analytical findings and for the qualitative analysis of the system's dynamics with and without impulse drug dosing.

Keywords: epithelial cell; antibody response; basic reproduction number; transcritical bifurcation; impulsive control; drug holidays

1. Introduction

The Coronavirus is considered to extend mainly between people who are close in touch with one another within about six feet and also through respiratory droplets created when an infected person coughs or sneezes. These droplets can enter the mouths or noses of people close by or possibly be inhaled into the lungs. Virus spreading depends on the possibility of touching virus-infected surfaces or objects and then touching their own mouth, nose, or possibly the eyes though. People are assumed to be most infectious when they are most indicative. [1].

Some renowned Mathematicians cum Scientists have gained their impressions in the diffused ways to fight against COVID-19 from the mathematical point of view. Joydev Chattopadhyay et al. [2] have discussed the short-term dynamics and preventive approaches for COVID-19. They have shown the declining inclination of new COVID-19 cases are well detained by their model for all the five provinces of China, namely, Hubei, Guangdong, Henan, Zhejiang, and Hunan. They have also established that effective management of quarantined persons is more flourishing than management of isolated persons to diminish the disease load. Malay Banerjee et al. [3] have attempted to measure quarantine strategies' efficiency by using their mathematical modeling. They have initiated a new model of infection progression, assuming that all infected persons are secluded after the incubation period. Their analysis has proved that the peak of

 doi:10.20944/preprints202209.0090.v1

infection (maximum of daily cases) is accomplished about ten days after the confined process is commenced. In this period, the growth rate of the total number of infected was increasingly lessening though the growth rate remains exponential in Italy. They have suggested that the introduced quarantine is not adequate and stricter measures are radically obligatory.

The transmission dynamics of COVID-19 at the population level in a different region of the world have been studied by researchers [4–9]. These studies mainly focused on susceptible populations, exposed populations, asymptomatic populations, and infected populations for a particular region. Recently Chatterjee et al. [10] proposed a model to find vaccination awareness to control the COVID-19 infection. It is also observed that every region has a different basic reproduction number (R_0) [9]. Thus the mortality rate varies for different regions. Population density is a major factor for disease transmission for this type of modeling. However, the micro-level (within-host) dynamical study of SARS-CoV-2 infection can give an insight look to the control of the virus in human host [11–13]. Infectious disease dynamics can be explored extensively with the help of mathematical modeling with real data [14–17] under cellular level. Tang et al. [18] proposed a four dimension host cell infection model for MARS-CoV mediated by DPP4 receptors. The infection process of SARS-CoV-2, SARS-CoV, and MARS-CoV are almost identical. Mathematicians are still working on inter-host modeling for SARS-CoV-2 and target cell limitation under immune responses. Chatterjee and Basir [19] formulate the dynamic model of the dynamics of epithelial cells during SARS- CoV-2 infection and CTL responses. They established a new mathematical model considering epithelial cells and the role of the ACE2 receptor using the impulsive differential equations, which describe the within-host dynamics of SARS-CoV-2 infection with treatments.

In the present article, we have explored the immunostimulant drug dynamics with the help of impulsive differential equations. Hernandez et al. [20] proposed a model to examine the cellular level dynamics and T cell responses against viral replication. Wang et al. evaluate the effect of several potential interventions for SARS-CoV-2. Their study reveals that combining the antiviral drug with interferon effectively reduces the viral plateau phase and shortens the recovery time. Chatterjee and Bashir [17] formulate a mathematical model to examine the consequence of adaptive immune response to the viral mutation to control disease transmission. They also study the effect of the combination of antiviral drug therapy and its impact on the model dynamics. Chatterjee et al. [13] proposed a set of Fractional differential equation models considering uninfected epithelial cells, infected epithelial cells, SARS-CoV-2 virus, and CTL response cells accounting for the lytic and non-lytic effects of immune responses. They also study the impact of a commonly used antiviral drug in COVID-19 treatment in an optimal control-theoretic approach. The role of innate and adaptive immune response for SARS-CoV-2 infection was also studied through mathematical modeling [13]. Wang et al. [16] studied the effect of antiviral drugs against SARS-CoV-2 viral dynamics during COVID-19 infection.

Proposing a mathematical model using impulsive differential equations, in this study, we study the target cell limited model of SARS-CoV-2 infection by examining the interaction between viral replication. We consider the uninfected virus target epithelial cells, infected epithelial cells, SARS-CoV-2 virus, and antibody responses. Our primary focus is to reduce the infected epithelial cell and viral load. A SARS-CoV-2 infected human being, the innate and adaptive immune responses work together to neutralize the threat of SARS-CoV-2 infection [21–23]. When the virus enters the human body, immediately the innate immune response starts spontaneously. Proteins of the natural immune system in a healthy cell also respond against the invading pathogens within the first minutes or hours of infection [24]. This response is of great importance in preventing new infections during the activation of the adaptive immune system [25]. Cytokines, which are small soluble proteins, are an essential component of the immune system [26]. They are secreted from different cells in the human body. They can be categorized into

Preprints (www.preprints.org) | NOT PEER-REVIEWED | Posted: 6 September 2022 doi:10.20944/preprints202209.0090.v1

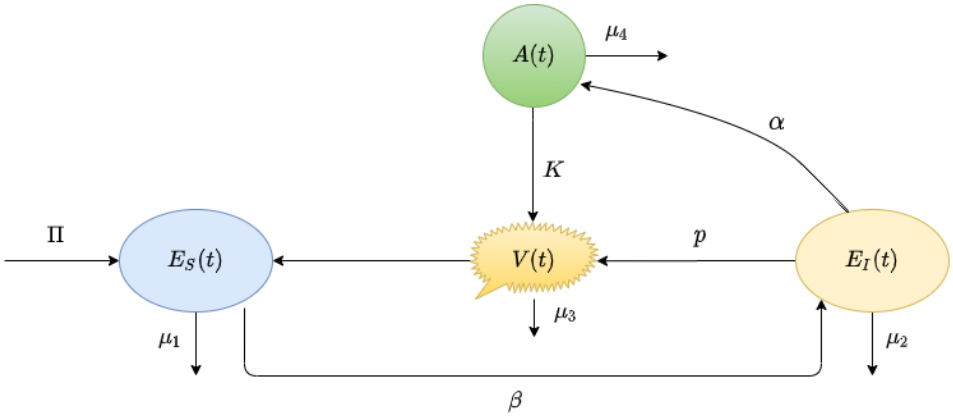

Figure 1. Conceptual diagram the mathematical model system (2) is presented. It is showing the flowchart of antibody responses in SARS-CoV-2 infection within a host.

one of four families: (i) the hematopoietic, (ii) the immunoglobin superfamily, (iii) the tumor necrosis factor family, and (iv) the interferon (IFN). The cytokine balances the innate and adaptive immune responses. Among the cytokines, IFN plays a vital role in the innate immune response during viral infection. Thus we consider the effect of adaptive immune responses in our mathematical model.

Despite numerous therapeutic strategies, to date, there is no specific effective treatment for SARS-CoV-2 infection. Recently all over the world, clinicians have been working on an effective therapy for coronavirus disease 2019 (COVID-19). It is observed that higher stirring cytokines have been reported in patients with COVID-19. Clinical observation suggests that cytokine levels enhance the hyperinflammatory response secondary to SARS-CoV-2 infection. These are the leading causes of multi-organ damage for COVID-19 patients. Due to these reasons, numerous clinical trials are currently undergoing to explore the effectiveness of the drugs such as interleukin-1 blockers and interleukin-6 inhibitors in COVID-19. The most modern method to study drug dynamics is determined by the use of impulsive differential equations [16]. Perfect or imperfect drug adherence and drug holidays can make easy the development of resistance. Recently, the effects of perfect drug dosing on antiretroviral therapy have been studied by impulsive differential equations. The dosing period and threshold values of dosage can be obtained using this method. Also, the effect of maximal acceptable drug holidays can be found by using impulsive differential equations [27].

The article is organized as follows. The very next section (section 2) contains the formulation of a target cell-limited mathematical model under immune responses. The qualitative properties of the model have been provided in Section 3. Theoretical analysis of the impulsive model is carried out in Section 4. The numerical simulation is included based on the analytical findings in section 5 outcomes. And the discussion and concluding remarks are given in Section 6.

2. Derivation of the mathematical model

The mathematical model helps us to understand the basic dynamics of viral infection. In general cases, modeling consist of a target cell limited model with some variants [28]. Here we consider the simplest version includes three populations, namely:

- $E_S(t)$: the uninfected susceptible target cell which is surface epithelial cells with ACE-2 receptor located at the respiratory tracks including lungs, nasal and trachea/ bronchial tissues,
- $E_I(t)$: the SARS-CoV-2 infected virus-producing cells,
- $V(t)$: the virus particles.

Preprints (www.preprints.org) | NOT PEER-REVIEWED | Posted: 6 September 2022 doi:10.20944/preprints202209.0090.v1

The SARS-CoV-2 dynamics with target cell limited model is proposed in [28], as the following

$$\begin{aligned} \frac{dE_S}{dt} &= \Pi - \beta E_S V - \mu_1 E_S, \\ \frac{dE_I}{dt} &= \beta E_S V - \mu_2 E_I, \\ \frac{dV}{dt} &= pE_I - \mu_3 V. \end{aligned} \tag{1}$$

The first equation of (1) shows the dynamics of uninfected epithelial cells ($E_S(t)$), the second equation shows the dynamics of the infected epithelial cells ($E_I(t)$). The replication of SARS-CoV-2 virus ($V(t)$) in the third equation of (1) is considering as SARS infection promotes the endothelins on several organs as a direct consequence of viral involvement [20].

The growth rate of epithelial cell is denoted as Π. Virus infect the uninfected cells with a rate β ((copies/ml) $^{-1}$day $^{-1}$). After the cell becomes infected it behaves like virus-producing cells and produces virus at a rate p (copies /ml/day^{-1} cell^{-1}) and virus particle cleared at a rate μ_3 (day^{-1}). The uninfected susceptible cells are cleared at a rate μ_1 (day^{-1}) due to their natural apoptosis and the infected cells are removed from the system at a rate μ_2 (day^{-1}) as a result of cytopathic viral effects and immune response [20].

Cytokine is vital in inhibiting viral replication and modulating downstream effects of the immune response. Specific cytokine activates natural killer cells (NK) which act against virally infected cells. In the case of SARS-CoV-2 infection, it is observed that viruses often target the JaK/STAT pathway (i.e. a chain of interactions between proteins in a cell) to decrease the production of IFNs. This immune suppressing mechanism is observed in SARS-CoV-2 can be represented in a functional form of a decrease in the cytokine production rate is assumed to be $\frac{\alpha E_I}{V+\theta}$. Cytokine activates the adaptive immune system mainly T cells and B lymphocytes to produce an antibody that acts against the virus. B cells mainly secrete IgM and IgG antibodies that are released from blood and lymph fluid and neutralize the SARS-CoV-2 viral particles.

Considering the antibody responses $A(t)$ we extend the target cell limited model including the depletion of virus modeled via the term rAV. The extended model of (1) reads as follows

$$\begin{cases} \frac{dE_S}{dt} = \Pi - \beta E_S V - \mu_1 E_S, \\ \frac{dE_I}{dt} = \beta E_S V - \mu_2 E_I, \\ \frac{dV}{dt} = pE_I - \mu_3 V - rVA, \\ \frac{dA}{dt} = \frac{\alpha E_I}{V+\theta} - \mu_4 A, \end{cases} \tag{2}$$

The graphical representation of the above is shown in Figure 1.

Here r is the rate at which the antibody neutralizes the viral particles, α is the antibody simulation rate constant and θ is the strength of immune suppression rate at which the antibody responses lost at a rate of μ_4.

Now we impose the impulsive drug dosing in the above model and analyse it analytically in section 4.

Impulsive differential equations result if drug effect as well as that of the metabolites are assumed to decay with time in an exponential manner during each cycle and are assumed to change instantaneously at dosing times, t_j for different drug doses and can result in either implicit or explicit models. In presence of antibody controlled therapy

Preprints (www.preprints.org) | NOT PEER-REVIEWED | Posted: 6 September 2022 doi:10.20944/preprints202209.0090.v1

Table 1: List of parameters for the model (4) [16].

Parameters	Short description	Range of value	Value taken
Π	Growth rate of epithelial cells	2 – 20	5
μ_1	Natural death rate uninfected epithelial cells	0.1 – 0.6	0.2
μ_2	Blanket death rate of infected epithelial cells	0.12 – 0.35	0.189
β	Rate of infection	0.00001 – 0.0019	0.0001
p	Growth rate of virus in cells	10 -140	70
μ_3	Virus clearance rate	0.10 – 0.41	0.1
α	Rate of antibody response from immune cells	0.3 – 1	0.4
r	The simulation rate	0.018 – 0.7	0.02
θ	Half maximal simulation threshold	0.01 – 0.4	0.1
μ_4	Antibody clearance rate	0.10 – 0.41	0.1

through perfect adherence, we consider the model system (2). Before analysing the system, we first discuss the one dimensional impulse system as follows:

$$\begin{aligned}
\frac{dE_S}{dt} &= \Pi - \beta E_S V - \mu_1 E_S, \\
\frac{dE_I}{dt} &= \beta E_S V - \mu_2 E_I, \\
\frac{dV}{dt} &= pE_I - \mu_3 V - rVA, \\
\frac{dA}{dt} &= \frac{\alpha E_I}{V+\theta} - \mu_4 A, \quad t \neq t_n. \\
A(t_n^+) &= \omega + A(t_n^-), \qquad\qquad t = t_n.
\end{aligned} \tag{3}$$

$A(t_n^-)$ denotes the CTL responses immediately before the impulse drug dosing, $A(t_n^+)$ denotes the concentration after the impulse and ω is the dose that is taken at each impulse time t_n, $k \in \mathbb{N}$.

3. Dynamics of the model without impulses

For the simplicity of analytical analysis, we reduce the four-population-model (2) by considering the quasi-steady-state approximation of the last equation of system (2) to a thee-population-model. Thus our reduced model becomes

$$\begin{cases}
\frac{dE_S}{dt} = \Pi - \mu_1 E_S - \beta V E_S, \\
\frac{dE_I}{dt} = \beta V E_S - \mu_2 E_I, \\
\frac{dV}{dt} = pE_I - \left(\mu_3 + \frac{kE_I}{V+\theta}\right) V,
\end{cases} \tag{4}$$

with the initial condition

$$E_S(0) = E_S^0,\ E_I(0) = E_I^0,\ V(0) = V^0. \tag{5}$$

Thus we replace the virus removal rate μ_3 with $\mu_3(E_I, V) = \mu_3 + \frac{kE_I}{V+\theta}$. The saturation function $\frac{kE_I}{V+\theta}$ where $k = r\frac{\alpha}{\mu_4}$ which fluctuations between 0 (before infection) to a maximum value α.

3.1. Nonnegativity and boundedness

In this section we investigate the nonnegativity of the state variables of the model (4) for all time t with initial condition $(E_S(0), E_I(0), V(0)) \in \mathbb{R}^3_+$. To prove the nonnegativity property, we establish the following theorem.

Theorem 1. *The system* (4) *with the initial values* (5) *satisfy* $E_S(t) > 0$, $E_I(t) > 0$, $V(t) > 0$ *for all* $t > 0$, *then the system* (4) *is positively invariant.*

Proof. The first equation of the model (4) can be rewritten as

$$\begin{aligned} \frac{dE_S(t)}{dt} &= \Pi - \beta E_S(t)V(t) - \mu_1 E_S(t), \\ &= \Pi - \xi_1 E_S(t), \end{aligned} \tag{6}$$

where $\xi_1 = \beta V(t) + \mu_1$. Integrating (6), we get

$$E_S(t) = E_S(0)\exp(-\int_0^t \xi_1(u)du) + \Pi\exp(-\int_0^t \xi_1(u)du \int_0^t (e^{\int_0^t \xi_1(v)dv})du) > 0. \tag{7}$$

This implies that $E_S(t)$ is nonnegative for all t. For the second equation of the system (4) we have

$$\frac{dE_I(t)}{dt} \geq -\mu_2 E_I(t),$$

which gives

$$E_I(t) = E_I(0)\exp(-\int_0^t \mu_2 du) > 0. \tag{8}$$

Similar way, for the last equation we can say that

$$\begin{aligned} \frac{dV(t)}{dt} &= rE_I(t) - \Big(\mu_3 + \frac{kE_I(t)}{V(t)+\theta}\Big)V(t), \\ &> -\xi_2 V(t), \end{aligned} \tag{9}$$

where $\xi_2 = \mu_3 + \frac{kE_I(t)}{V(t)+\theta}$. Therefore,

$$V(t) = V(0)\exp(-\int_0^t \xi_2(u)du) > 0. \tag{10}$$

The above results show that all the solution trajectories of the system (4) are non-negative for all $t > 0$. □

To verify the boundedness of the system (4) with non-negative initial values, we have the following theorem.

Theorem 2. *The system* (4) *with the initial condition* (5) *are uniformly bounded in the positive invariant set* $\mathcal{U}$, *where*

$$\mathcal{U} = \Big\{(E_S(t), E_I(t), V(t)) \in \mathbb{R}^3_+ | 0 \leq E \leq \frac{\Pi}{\mu_1}, 0 \leq V(t) \leq \frac{p\Pi}{\mu_1\mu_3}\Big\}. \tag{11}$$

Proof. From the positively of the solution, we get

$$\begin{aligned} \frac{dE_S(t)}{dt} &= \Pi - \mu_1 E_S(t) - \beta E_S(t)V(t), \\ &\leq \Pi - \mu_1 E_S. \end{aligned} \tag{12}$$

Preprints (www.preprints.org) | NOT PEER-REVIEWED | Posted: 6 September 2022 doi:10.20944/preprints202209.0090.v1

This implies that

$$\lim_{t\to\infty} \sup E_S(t) \leq \frac{\Pi}{\mu_1}. \tag{13}$$

Now, $E(t) = E_S(t) + E_I(t)$ then

$$\begin{aligned} \frac{dE(t)}{dt} &= \Pi - \mu_1 E_S(t) - \mu_2 E_I(t), \\ &\leq \Pi - \mu_1 (E_S(t) + E_I(t)) \text{ as } \mu_1 < \mu_2, \\ &\leq \Pi - \mu_1 E(t). \end{aligned} \tag{14}$$

Hence, we can write $\lim_{t\to\infty} \sup E(t) \leq \frac{\Pi}{\mu_1}$.

Also from the third equation of (4), we have

$$\begin{aligned} \frac{dV(t)}{dt} &= pE_I(t) - \Big(\mu_3 + \frac{kE_I(t)}{V(t)+\theta}\Big)V(t), \\ &\leq \frac{p\Pi}{\mu_1} - \Big(\mu_3 + \frac{kE_I(t)}{V(t)+\theta}\Big)V(t), \\ &\leq \frac{p\Pi}{\mu_1} - \mu_3 V(t), \\ \implies \lim_{t\to\infty} \sup V(t) &\leq \frac{p\Pi}{\mu_1\mu_3}. \end{aligned} \tag{15}$$

Therefore, all the solution trajectories that start from $\mathbb{R}^3_+$ will enter the region $\mathcal{U}$ and never leave it. □

3.2. The Basic Reproduction number

The next-generation matrix method is introduced by Driessche, Pauline, and Watmough in [29] is used to determine the basic reproduction number. For this purpose, we consider the non-negative matrix $\mathcal{G}$ and non-negative M matrix $\mathcal{H}$ which represents the production of the new infection, and another one is the transportation part respectively. The target cell viral dynamical system of (4) is defined below:

$$\mathcal{G} = \begin{pmatrix} \beta E_S V \\ 0 \end{pmatrix}, \ \mathcal{H} = \begin{pmatrix} \mu_2 E_I \\ -pE_I + \Big(\mu_3 + \frac{kE_I}{V+\theta}\Big)V \end{pmatrix}. \tag{16}$$

Now the matrix **G** and **H** can be written as

$$\mathbf{G} = \Big[\frac{\partial \mathcal{G}_i}{\partial x_j}(\bar{P})\Big], \ \mathbf{H} = \Big[\frac{\partial \mathcal{H}_i}{\partial x_j}(\bar{P})\Big], \text{with, } 1 \leq i, j \leq 2. \tag{17}$$

Also, **G** is non-negative and **H** is non-singular M matrix and all eigenvalues of J_3 have positive real parts.

At the Disease free equilibrium ($\bar{P}$) the matrix C and H are defined as

$$\mathbf{G} = \begin{bmatrix} 0 & \beta E_S \\ 0 & 0 \end{bmatrix}_{\bar{P}} = \begin{bmatrix} 0 & \frac{\beta\Pi}{\mu_1} \\ 0 & 0 \end{bmatrix}. \tag{18}$$

Therefore the basic reproduction number, denoted by R_0, is the spectral radius of the next generation matrix, is obtained as

$$R_0 = \rho(\mathbf{G}\mathbf{H}^{-1}) = \frac{p\beta\Pi}{\mu_1\mu_2\mu_3}. \tag{19}$$

Preprints (www.preprints.org) | NOT PEER-REVIEWED | Posted: 6 September 2022 doi:10.20944/preprints202209.0090.v1

3.3. Existence of equilibrium points

The system (4) has two equilibria: (i) the disease-free equilibrium $\bar{P}(\frac{\Pi}{\mu_1}, 0, 0)$ exist, and (ii) the endemic equilibrium point $P^*(E_S^*, E_I^*, V^*)$, where,

$$E_S^* = \frac{\Pi}{\beta V^* + \mu_1}, \; E_I^* = \frac{\Pi \beta V^*}{\mu_2(\beta V^* + \mu_1)}, \tag{20}$$

and V^* is defined as

$$b_0 V^{*2} + b_1 V^* + b_2 = 0, \tag{21}$$

where,

$$\begin{aligned} b_0 &= \mu_2 \mu_3 \beta, \\ b_1 &= \mu_2 \mu_3 (\mu_1 + \beta\theta) + \beta\Pi(k - p), \\ b_2 &= \theta \mu_1 \mu_2 \mu_3 (1 - R_0). \end{aligned} \tag{22}$$

We have the Theorem

Theorem 3. *When $R_0 > 1$, one and only one endemic equilibrium P^* exist. For $R_0 < 1$, there may exists two endemic points for $R_0 < 1$.*

Proof. From the equation (21) it is clear that $b_0 > 0$ and $b_2 > 0$ if $R_0 < 1$. Also if $R_0 > 1$ then $b_2 < 0$. Using Descartes Rule of signs, we can say that there exist a unique endemic equilibrium if $b_2 < 0$ and two positive endemic equilibrium if $b_2 > 0$, $b_1 < 0$, and $b_1^2 - 4b_0 b_2 > 0$. □

Remark 1. *Moreover, a transcritical bifurcation occurs when $b_2 = 0$ i.e. $R_0 = 1$ and $b_1 < 0$ with $b_1^2 - 4b_0 b_2 = 0$ (i.e. the point where two positive endemic equilibrium coincide each other and leaving the stable disease-free equilibrium point.)*

3.4. Stability of Equilibrium points

In this section, we have discussed the local and global stability of the equilibrium points.

For the stability of disease-free equilibrium, we have the following theorem.

Theorem 4. *The disease free equilibrium $\bar{P}(\frac{\Pi}{\mu_1}, 0, 0)$ is locally asymptotically stable for $R_0 < 1$ and when $R_0 > 1$ the disease-free system becomes unstable.*

Proof. To verify the locally asymptotically stability at $\bar{P}$, we compute the Jacobian matrix of (4) around $\bar{P}$ is given below

$$J_{\bar{P}} = \begin{pmatrix} -\mu_1 & 0 & -\frac{\beta\Pi}{\mu_1} \\ 0 & -\mu_2 & \frac{\beta\Pi}{\mu_1} \\ 0 & p & -\mu_3 \end{pmatrix}. \tag{23}$$

According to the Cayley-Hamilton Theorem, we get the characteristic equation from $\det(J_{\bar{P}} - \lambda I_3) = 0$. By solving the characteristic equation we get the eigenvalues $-\mu_1$ and other two eigenvalues can be obtained from the equation

$$\lambda^2 + a_1 \lambda + a_2 = 0 \tag{24}$$

where $a_1 = \mu_2 + \mu_3$, $a_2 = \mu_1 \mu_2 \mu_3 (1 - R_0)$. Here $a_1 = \mu_2 + \mu_3 > 0$ and $a_2 > 0$ if $R_0 < 1$ which suggest that all two roots are negative real roots or with negative real parts. Hence

Preprints (www.preprints.org) | NOT PEER-REVIEWED | Posted: 6 September 2022 doi:10.20944/preprints202209.0090.v1

the disease free equilibrium is locally asymptotically stable if $R_0 < 1$ and unstable if $R_0 > 1$. □

We have already proved that when $R_0 < 1$ the disease free equilibrium $\bar{P}$ is locally asymptotically stable. Now we verity the global stability of $\bar{P}$. For this purpose, we construct the Lyapunov function following [30,31]. We have the following theorem for the global stability of $\bar{P}$.

Theorem 5. *The disease free equilibrium $\bar{P}$ is globally asymptotically stable if $R_0 < 1$ and it is unique equilibrium. Otherwise $\bar{P}$ is unstable and a unique endemic equilibrium P^* exist.*

The proof of the theorem 5 is provided in the **Appendix G**.

Now we analyse transcritical bifurcation between the disease-free and the endemic equilibrium points. We have the following theorem for this analysis.

Theorem 6. *The system exhibits backward transcritical bifurcation when $R_0 = 1$ for $p > p^c$ and shows forward bifurcation for $p < p^c$, where p^c is defined in the proof.*

Proof. To prove the Theorem we use the approach used by Castillo-Chavez and Song, 2004 [32] for applying the centre manifold theory to analyze the dynamics of the system (4). The model variable of the system (4) are transformed as $x_1 = E_S$, $x_2 = E_I$, $x_3 = V$ and the total population $n = \sum_{i=1}^{3} x_i$. Now we define $X = (x_1, x_2, x_3)^T$ such that the model (4) can be rewritten as $\frac{dX}{dt} = F(x)$, where $F = (f_1, f_2, f_3)$. Hence the model (4) becomes:

$$\begin{cases} f_1 = & \frac{dx_1}{dt} = \Pi - \beta x_1 x_3 - \mu_1 x_3, \\ f_2 = & \frac{dx_2}{dt} = \beta x_1 x_3 - \mu_2 x_2, \\ f_3 = & \frac{dx_3}{dt} = p x_2 - \left(\mu_3 + \frac{k x_2}{x_3 + \theta}\right) x_3. \end{cases} \tag{25}$$

At $R_0 = 1$, we choose the bifurcation parameter $\tilde{\beta}$ such that

$$\tilde{\beta} = \beta^* = \frac{\mu_1 \mu_2 \mu_3}{\Pi p}. \tag{26}$$

Then the Jacobian matrix of the equation (25) at the disease free equilibrium $\bar{P}$ is given by

$$J_{\bar{P}} = \begin{pmatrix} -\mu_1 & 0 & -\frac{\beta^* \Pi}{\mu_1} \\ 0 & -\mu_2 & \frac{\beta^* \Pi}{\mu_1} \\ 0 & p & -\mu_3 \end{pmatrix}, \tag{27}$$

with $\beta = \beta^*$, the transformed system (25) has a hyperbolic equilibrium point.

The eigenvalues of the $J_{\bar{P}}$ are $-\mu_1, 0$ and $-(\mu_2 + \mu_3)$. Here other than 0 all eigenvalues have negative real parts. By applying the centre manifold Theorem we get the left and right eigenvectors corresponding to the zero eigenvalue. Let the left hand eigenvector and the right hand eigenvector of the Jacobian matrix $J_{\bar{P}}$ are denoted as $s = (s_1, s_2, s_3)$ and $t = (t_1, t_2, t_3)^T$ which are given by

$$\begin{aligned} s &= \left[\frac{\beta^* \Pi}{\mu_1}, \frac{\beta^* \Pi}{\mu_1 \mu_2}, 1\right] s_3, \ \ s_3 > 0, \\ t &= [0, \frac{p}{\mu_2}, 1]^T t_3, \ \ t_3 > 0, \end{aligned} \tag{28}$$

Preprints (www.preprints.org) | NOT PEER-REVIEWED | Posted: 6 September 2022 doi:10.20944/preprints202209.0090.v1

where T denotes the transpose of a matrix. Now we assume the bifurcation parameter a and b defined as

$$\begin{aligned} a &= \sum_{k,i,j=1}^{3} s_n t_i t_j \frac{\partial^2 f_n}{\partial x_i \partial x_j}, \\ b &= \sum_{k,i=1}^{3} s_n t_i \frac{\partial^2 f_n}{\partial x_i \partial \beta^*}. \end{aligned} \tag{29}$$

To calculate the bifurcation parameter a and b we consider only nonzero partial derivatives of the model (25) at disease-free equilibrium. The results are given below

$$\begin{aligned} \frac{\partial^2 f_1}{\partial x_1 \partial x_3}(\bar{P}) &= -\beta^*, \\ \frac{\partial^2 f_2}{\partial x_1 \partial x_3}(\bar{P}) &= \beta^*, \\ \frac{\partial^2 f_3}{\partial x_2 x_3}(\bar{P}) &= -\frac{k}{\theta^2}, \end{aligned} \tag{30}$$

so that

$$\begin{aligned} a &= t_1 s_1 s_3 \frac{\partial^2 f_1}{\partial x_1 \partial x_3}(\bar{P}) + t_2 s_1 s_3 \frac{\partial^2 f_2}{\partial x_1 \partial x_3}(\bar{P}) + t_3 s_2 s_3 \frac{\partial^2 f_3}{\partial x_2 \partial x_3}(\bar{P}), \\ &= \frac{\beta^2 \Pi}{\mu_1 \mu_2 \mu_3}(p - p^c) t_3 s_3^2, \end{aligned} \tag{31}$$

where

$$p^c = \frac{k\mu_1}{\beta\theta^2}. \tag{32}$$

Also the nonzero partial derivatives associates with b is given below

$$\begin{aligned} \frac{\partial^2 f_1}{\partial x_3 \partial \beta^*}(\bar{P}) &= -\frac{\Pi}{\mu_1}, \\ \frac{\partial^2 f_2}{\partial x_3 \partial \beta^*}(\bar{P}) &= \frac{\Pi}{\mu_1}, \end{aligned} \tag{33}$$

so that

$$\begin{aligned} b &= t_1 s_3 \frac{\partial^2 f_1}{\partial x_3 \partial \beta^*}(\bar{P}) + t_2 s_3 \frac{\partial^2 f_2}{\partial x_3 \partial \beta^*}(\bar{P}), \\ &= \frac{p\Pi}{\mu_1 \mu_2} t_3 s_3 > 0. \end{aligned} \tag{34}$$

The system (4) switches its stability at its transcritical bifurcation point $R_0 = 1$. Here one of the bifurcation coefficient $a > 0$ if $p > p^c$ which implies that the system (4) will enter into the bistability regions where there exists two endemic equilibrium when $R_0 < 1$ which is called backward bifurcation. But the system switches towards forward bifurcation if $p < p^c$ at $R_0 = 1$. This type of bifurcation suggests that at $R_0 = 1$ the reinfection occurs due to some external factor when viral production rate p exceeds its certain critical value denoted as p^c. □

Remark 2. *In case of reinfection, the global stability of the endemic equilibrium P^* is not guaranteed when $R_0 > 1$, this is due to some external factors. In the next subsection, we deals with the global stability of the system (4) at the endemic equilibrium point P^* when $R_0 > 1$.*

Preprints (www.preprints.org) | NOT PEER-REVIEWED | Posted: 6 September 2022 doi:10.20944/preprints202209.0090.v1

Now we study the stability of P^*. For this we calculate the Jabian matrix as

$$J_{P^*} = \begin{pmatrix} -\mu_1 - \beta V^* & 0 & -\beta E_S^* \\ \beta V^* & -\mu_2 & \beta E_S^* \\ 0 & p - \frac{kV^*}{V^*+\theta} & -\mu_3 - \frac{k\theta E_I^*}{(V^*+\theta)^2} \end{pmatrix}, \tag{35}$$

The characteristic at the endemic equilibrium P^* is

$$\rho^3 + \sigma_1\rho^2 + \sigma_2\rho + \sigma_3 = 0. \tag{36}$$

where,

$$\sigma_1 = \mu_1 + \mu_2 + \mu_3 + \beta V^* + \frac{k\theta E_I^*}{(V^*+\theta)^2},$$
$$\sigma_2 = \mu_2(\mu_3 + \frac{k\theta E_I^*}{(V^*+\theta)^2}) + (\mu_1 + \beta V^*)(\mu_3 + \frac{k\theta E_I^*}{(V^*+\theta)^2}) + \mu_2(\mu_1 + \beta V^*) - p\beta E_S^* + \frac{\beta k V^*}{V^*+\theta}$$
$$\sigma_3 = \beta E_S^*(p\beta E_S^* - \frac{\beta k V^*}{V^*+\theta}) + (\mu_1 + \beta V^*)(\mu_2(\mu_3 + \frac{k\theta E_I^*}{(V^*+\theta)^2}).$$

Clearly, $\sigma_1 > 0$. Thus using the Routh-Hurwitz criteria, we can say that the equilibrium P^* of model (4) is locally asymptotically stable if the relations are true,

$$\sigma_2 > 0,\ \sigma_3 > 0 \ \text{ and } \ \sigma_1\sigma_2 - \sigma_3 > 0. \tag{37}$$

Also, it is easy to verify that for $R_0 > 1$, the above conditions holds always. we have the following theorem from the above analysis.

Theorem 7. *For $R_0 > 1$, the endemic equilibrium point $P^*(E_S^*, E_I^*, V^*)$ is locally asymptotically stable.*

Now we analyse the global stability of the system (4) for the endemic equilibrium point P^* when $R_0 > 1$. To show this, we use a Dulac function. Now we prove Global stability of endemic equilibrium in the following theorem.

Theorem 8. *When $R_0 > 1$ the system (4) is globally asymptotically stable at the endemic equilibrium point P^*.*

The proof of the above theorem 8 is given in the **Appendix H**.

4. Dynamics of the system with impulsive drug dosing

For analysing the impulsive system (3), we first analyse the following linear impulsive system.

$$\begin{aligned} \frac{dA}{dt} &= -\mu_4 A, & t \neq t_n \\ \Delta A &= \omega, & t = t_n \end{aligned} \tag{38}$$

where, $\Delta = A(t_n^+) - A(t_n^-)$. Let $\tau = t_{k+1} - t_n$ be the period of the campaign. The solution of the system (38) is,

$$A(t) = A(t_n^+)e^{-\mu_4(t-t_n)}, \ \text{ for } \ t_n < t \leq t_{k+1}. \tag{39}$$

Preprints (www.preprints.org) | NOT PEER-REVIEWED | Posted: 6 September 2022 doi:10.20944/preprints202209.0090.v1

In presence of impulsive dosing, we can get the recursion relation at the moments of impulse as written below,

$$A(t_n^+) = A(t_n^-) + \omega.$$

Thus the amount of antibody responses before and after the impulse is obtained respectively as,

$$A(t_n^+) = \frac{\omega(1 - e^{-k\tau\mu_4})}{1 - e^{-\tau\mu_4}} \tag{40}$$

and

$$A(t_{k+1}^-) = \frac{\omega(1 - e^{-k\tau\mu_4})e^{-\tau\mu_4}}{1 - e^{-\tau\mu_4}}. \tag{41}$$

Thus the limiting case of the antibody responses before and after one cycle are

$$\lim_{k\to\infty} A(t_n^+) = \frac{\omega}{1 - e^{-\tau\mu_4}} \text{ and } \lim_{k\to\infty} A(t_{k+1}^-) = \frac{\omega e^{-\tau\mu_4}}{1 - e^{-\tau\mu_4}}$$

and

$$A(t_{k+1}^+) = \frac{\omega e^{-\tau\mu_4}}{1 - e^{-\tau\mu_4}} + \omega = \frac{\omega}{1 - e^{-\tau\mu_4}},$$

respectively.

We now require the following definitions and lemmas for this study [33,34]:

Definition 1. *Let $\Lambda \equiv (E_S, E_I, V, A)$, $B_0 = [B : R_+^4 \to R_+]$, then we say that B belong to class B_0 if the following conditions hold:*
(i) B is continuous on $(t_n, t_{k+1}] \times R_+^3, n \in N$ and for all $\Lambda \in R^4$,
$lim_{(t,\mu)\to(t_n^+,\Lambda)} B(t,\mu) = B(t_n^+, \Lambda)$ exists,
(ii) B is locally Lipschitzian in Λ.

Lemma 1. *Let $Z(t)$ be a solution of the system (3) with $Z(0^+) \geq 0$. Then $Z_i(t) \geq 0$, $i = 1, \ldots, 4$ for all $t \geq 0$. Coreover, $Z_i(t) > 0$, $i = 1, \ldots, 4$ for all $t > 0$ if $Z_i(0^+) > 0$, $i = 1, \ldots, 4$.*

Lemma 2. *There exists a constant γ such that $E_S(t) \leq \gamma$, $E_I(t) \leq \gamma$, $V(t) \leq \gamma$ $A(t) \leq \gamma$ for each and every solution $Z(t)$ of system (3) for all sufficiently large t.*

Lemma 3. *Let assume that $B \in B_0$ and also let*

$$D^+B(t, Z) \leq j(t, B(t, Z(t))), \quad t \neq t_n,$$
$$B(t, Z(t^+)) \leq \Phi_n(B(t, Z(t))), \quad t = t_n,$$

where $j : \mathbf{R}_+ \times \mathbf{R}_+ \to \mathbf{R}$ is continuous function in $(t_n, t_{k+1}]$ for $e \in \mathbf{R}_+^2$, $n \in N$, the limit $\lim_{(t,V)\to(t_n^+)} j(t, g) = j(t_n^+, x)$ exists and $\Phi_n^i (i = 1, 2) : \mathbf{R}_+ \to \mathbf{R}_+$ is non-decreasing. Let $y(t)$ be a maximal solution of the following impulsive differential equation

$$\begin{aligned} \frac{dx(t)}{dt} &= j(t, x(t)), \quad t \neq t_n, \\ x(t^+) &= \Phi_n(x(t)), \quad t = t_n, \quad x(0^+) = x_0, \end{aligned} \tag{42}$$

existing on $(0^+, \infty)$. Then $B(0^+, Z_0) \leq x_0$ implies that $B(t, Z(t)) \leq y(t)$, $t \geq 0$, for any solution $Z(t)$ of system (3). If j satisfies additional smoothness conditions to ensure the existence and uniqueness of solutions for (42), then $y(t)$ is the unique solution of (42).

The lemmas provided above, gives the following result,

Preprints (www.preprints.org) | NOT PEER-REVIEWED | Posted: 6 September 2022 doi:10.20944/preprints202209.0090.v1

Lemma 4. *System (38) has a unique positive periodic solution $\tilde{A}(t)$ with period τ and it can be written as*

$$\tilde{A}(t) = \frac{\omega\, exp(-\mu_4(t-t_n))}{1-exp(-\tau\mu_4)}, \quad t_n \le t \le t_{k+1}, \quad \tilde{A}(0^+) = \frac{\mu_4}{1-exp(-\tau\mu_4)}. \tag{43}$$

We use the result in Lemma 4, we establish the following theorem.

Theorem 9. *The disease-free periodic orbit $(\tilde{E_S}, 0, 0, \tilde{A})$ of the system (2) is locally asymptotically stable if*

$$\tilde{R_0} < 1 \tag{44}$$

where,

$$\tilde{R_0} = \frac{\mu_2}{p\beta\,\tau}\int_0^\tau \frac{(\mu_3 + r\tilde{A}}{\tilde{E_S}}dt.$$

Proof. Let the disease-free periodic solution of the system (3) be denoted by $\tilde{P}(\tilde{E_S}, 0, 0, \tilde{A})$, where

$$\tilde{A}(t) = \frac{\omega\ \exp(-\mu_4(t-t_n))}{1-\exp(-\tau\mu_4)}, \quad t_n \le t \le t_{k+1},$$

with initial condition $A(0^+)$ as in Lemma 4.

We now test the stability of the disease-free equilibrium point. The variational matrix $M(t)$ at disease-free periodic orbit $\tilde{P}(\tilde{T}, 0, 0, \tilde{E}, \tilde{C})$ is calculated as

$$M(t) = [m_{ij}] = \begin{pmatrix} -\mu_1 & 0 & 0 & -\beta\tilde{E_S} \\ 0 & -\mu_2 & \beta\tilde{E_S} & 0 \\ 0 & p & -\mu_3 - r\tilde{A} & 0 \\ 0 & \frac{\alpha}{\theta} & 0 & -\mu_4 \end{pmatrix}.$$

The monodromy matrix $\mathbb{P}$ of the variational matrix $M(t)$ is

$$\mathbb{P}(\tau) = I_n \exp\left(\int_0^\tau M(t)dt\right),$$

where I_n is the identity matrix.

The monodromy matrix can be rewritten as $\mathbb{P}(\tau) = \text{diag}(\sigma_1, \sigma_2, \sigma_3, \sigma_4)$, where, σ_i, $i = 1, 2, 3, 4$, are the Floquet multipliers, and they are determined as

$$\sigma_1 = \exp(-\mu_1\tau), \ \ \sigma_{2,3} = \exp\left(\int_0^\tau \frac{1}{2}\left[-A \pm \sqrt{A^2 - 4B}\right]dt\right),$$
$$\sigma_4 = \exp(-\mu_4\tau).$$

Here $A = \mu_2 + \mu_3 + \tilde{A}$ and $B = \mu_2(\mu_3 + \tilde{A}) - p\beta\tilde{E_S}$. It is noted that $\lambda_{1,4} < 1$. Also, we check that $A^2 - 4B > 0$. Now if $B \ge 0$ holds then we get $\lambda_{2,3} < 1$. Thus, according to Floquet theory, the disease-free periodic orbit $\tilde{P}(\tilde{E_S}, 0, 0, \tilde{A})$ of the system (3) is asymptotically stable if the conditions given in (44) is true. □

There is another periodic orbit $P(\tilde{E_S}, \tilde{E_I}, \tilde{V}, \tilde{A})$ of the impulsive system (3). We analyse its dynamics through numerical simulation.

In the above section, we discussed about the perfect drug dosing. Now we discuss the imperfect drug dosing in the following subsection.

Preprints (www.preprints.org) | NOT PEER-REVIEWED | Posted: 6 September 2022 doi:10.20944/preprints202209.0090.v1

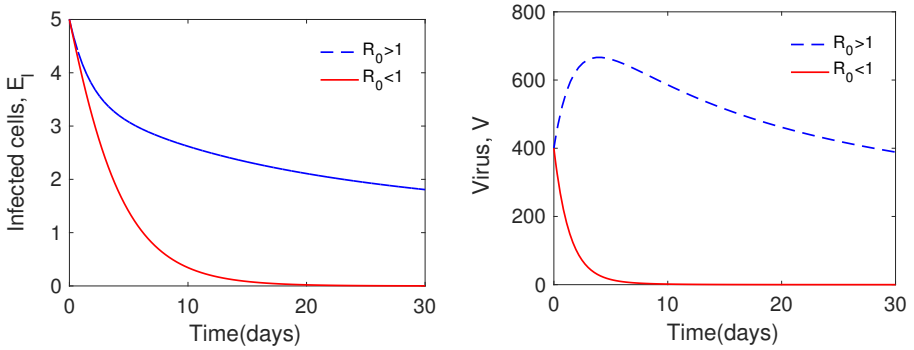

Figure 2. This figure shows that when $R_0 < 1$, the system attains its disease-free state and for $R_0 > 1$, the system attains its endemic state.

4.1. Impact of imperfect drug dosing

Suppose, a Covid-19 patient, during the treatment stage, takes a drug holiday after taking $n = n_1$ doses. Let us assume a positive quantity A_1, which denotes the minimum difference between the density of antibody after $n = n_1$ doses and normal concentration of antibody A_2.

Our consideration is based on the assumption that a patient usually misses his perfect drug dose when he achieves almost cured stage. Thus the covid-19 patients can take a drug holiday after taking n_1 doses when the difference between the antibody response after $n = n_1$ doses and normal threshold $\tilde{A}$, is less than a chosen small positive number, A_1. Thus we must have

$$A(t_{n_1}^{+}) \quad \geq \quad A_2 - A_1. \tag{45}$$

A patient may take a drug holiday once the antibody response reached a periodic orbit. Suppose h_1 doses are subsequently missed, then we impose the condition that the antibody response will reach a high level and patient can realize that the further treatment is highly needed.

Now we assume, the difference between the present antibody response and the possible maximum response of it, is less or equal to a small positive number (ϵ). So, the inequality $A(t_{n_1+h_1}^{-}) \geq A_{max} - \epsilon$, allow us to find the maximum number of doses a patient can miss.

Suppose a patient has missed h_1 doses. Now, in order to keep the antibody response above A_2 after n_2 doses are taken, a new condition must be applied that forces the antibody level to be A_3 away from the A_2. The condition is the the following that must be satisfied:

$$A(t_{n_1+h_1+n_2}^{+}) \quad \geq \quad A_2 - A_3. \tag{46}$$

From (46), n_2 can be determined. Nut the calculations for determining n_2 is complicated. One can see the article [35] for the detail analysis. We determine it from numerical simulations.

5. Numerical Simulation

In this section, we study the mathematical models (4) through numerical simulation. The data are taken mainly from Wolfel et al. [36], and some are estimated. The daily reported and measured viral load for patients was collected from a hospital in Munich, Germany. We have considered one data set for this study. The values of the model parameters applied in our numerical simulation are given in Table 1, and System dynamics are shown in the schematic diagram (Figure 1).

Preprints (www.preprints.org) | NOT PEER-REVIEWED | Posted: 6 September 2022 doi:10.20944/preprints202209.0090.v1

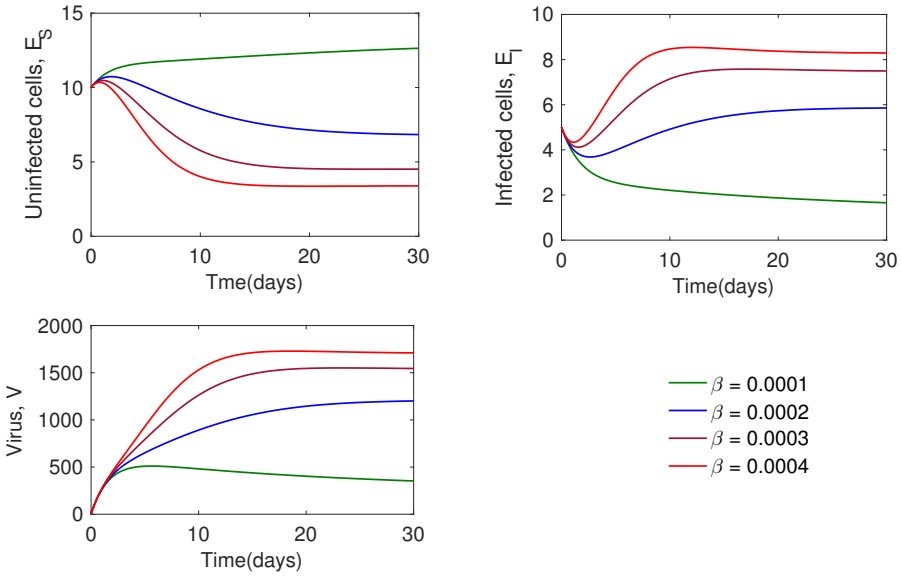

Figure 3. This figure shows the effect of model variables for varying β in which the system goes to more infected state.

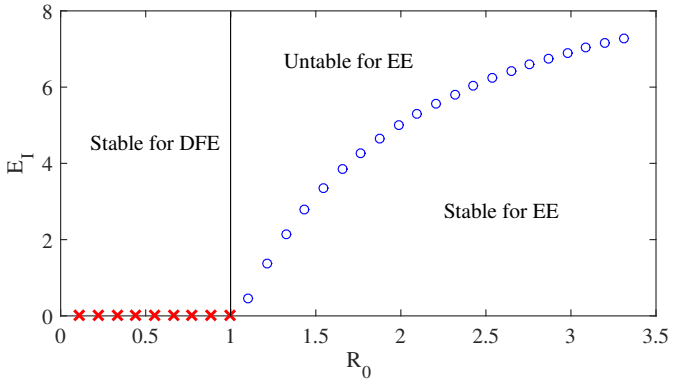

Figure 4. Backward (Left panel) and forward (Right panel) bifurcation diagram of system (4) using Theorem 7. Red and blue curves represent disease-free equilibria (DFE) and endemic equilibria (EE), respectively.

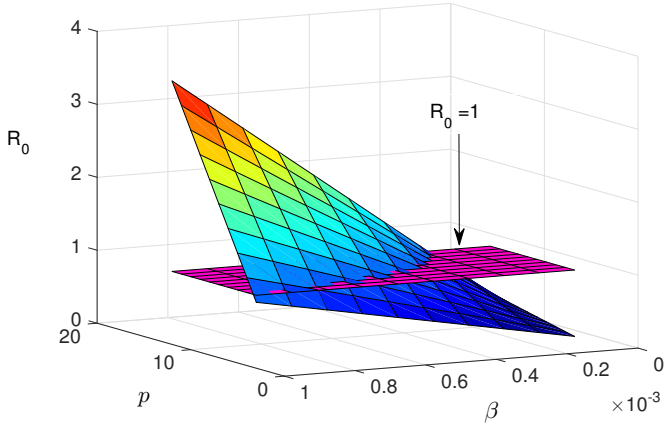

Figure 5. In this surface plot shows the effect of model variables with time for both β and p vary from lower to higher values and with disease free equilibrium $R_0 = 1$.

Preprints (www.preprints.org) | NOT PEER-REVIEWED | Posted: 6 September 2022 doi:10.20944/preprints202209.0090.v1

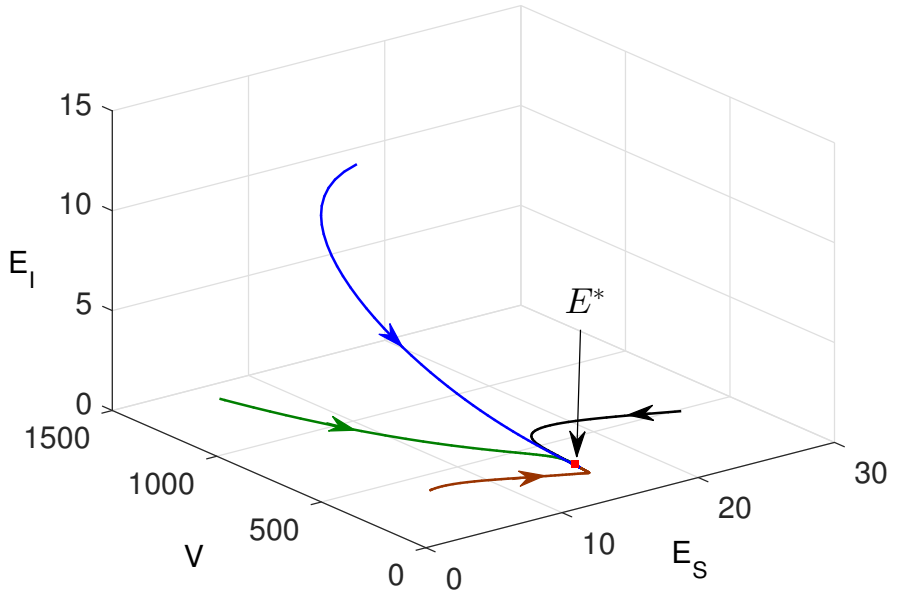

Figure 6. Phase portraits are plotted in $E_S - V - E_I$ phase space taking different initial conditions and $R_0 > 1$.

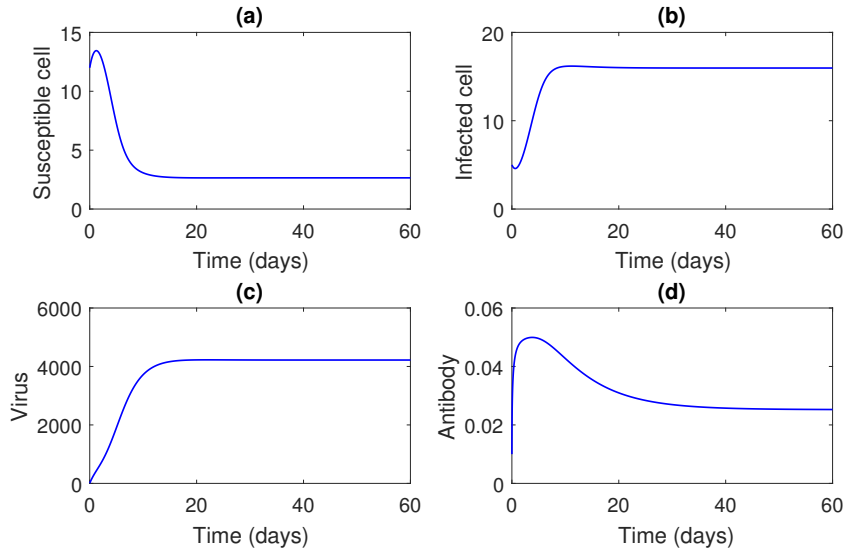

Figure 7. Solutions of the impulsive system 3 for $\omega = 0$ i.e. without drug dosing.

Preprints (www.preprints.org) | NOT PEER-REVIEWED | Posted: 6 September 2022 doi:10.20944/preprints202209.0090.v1

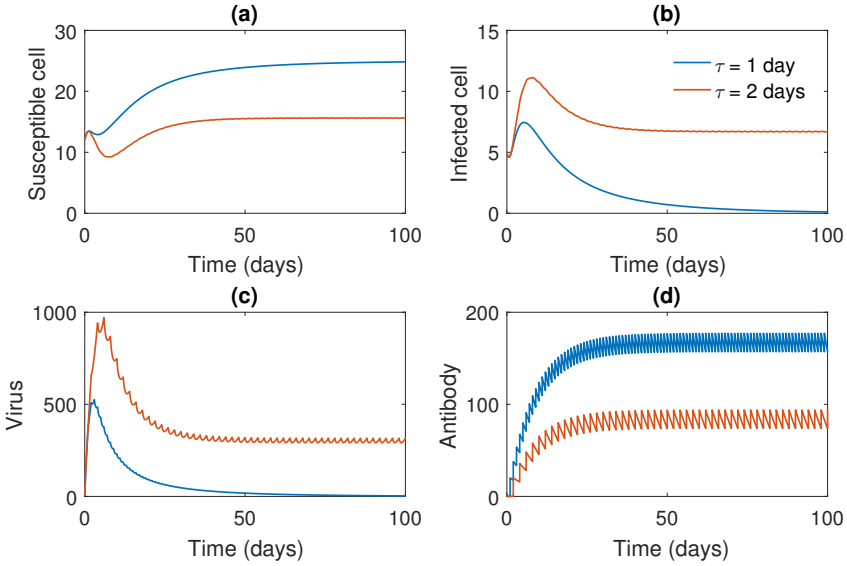

Figure 8. Solutions of the impulsive system 3 has been shown for of different impulse intervals ($\tau = 1, 2$) for drug dosing.

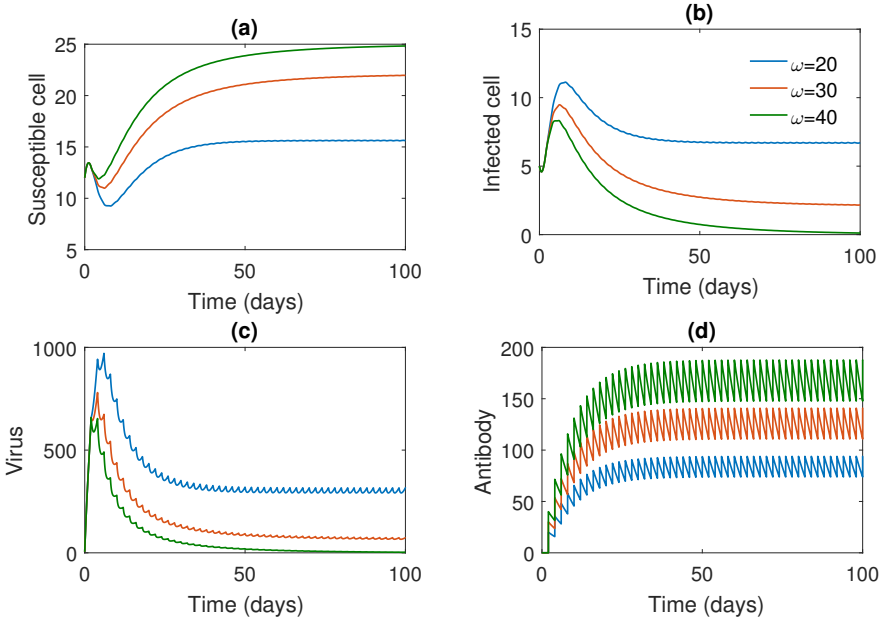

Figure 9. Numerical solutions of the impulsive system 3 for different dosing rates ($\omega = 20, 30, 40$) for fixed dosing interval $\tau = 2$ days.

Preprints (www.preprints.org) | NOT PEER-REVIEWED | Posted: 6 September 2022 doi:10.20944/preprints202209.0090.v1

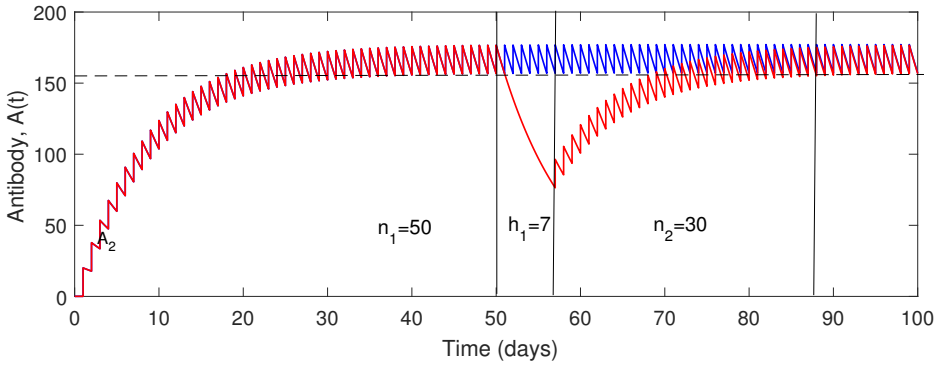

Figure 10. Solutions of the impulsive system 3 are plotted for a fixed interval ($\tau = 1$ day) and fixed drug dosing $\omega = 20$ taking tolerable drug holidays.

From Figure 2, it is clearly observed that the system changes its state from disease-free equilibrium to endemic equilibrium. If the basic reproduction number changes from $R_0 < 1$ to $R_0 > 1$, the system attains its endemic state, and the disease persists.

Figure 3 shows the Change of the model trajectories with time for different values of β. This figure displays that as the infection rate increases, the infected cell population and viral load also increase accordingly.

Figure 4 describes the forward bifurcation of system (4) by using the Theorem 6 and the parameters value in 1. Red and blue curves represent disease-free equilibrium and endemic equilibrium. When $R_0 = 1$ the large endemic equilibrium exists but the smaller one vanishes. Simultaneously, the disease-free state loses its stability. It can be observed that the disease-free equilibrium is stable when $R_0 < 1$ while the endemic equilibrium starts to rise with $R_0 > 1$ (Theorem 4).

Figure 5 represents a surface plot of the model parameters with time for both β and p increases from lower to higher values so that the disease equilibrium (R_0) goes to endemic state as ($R_0 > 1$).

Figure 6 shows that the phase trajectories converge to the same point (endemic equilibrium point) though the initial values are different. From this we can conclude that the endemic equilibrium is globally asymptotically stable.

Simulations results of the impulsive system has been plotted in Figure **??** and Figure **??**.

Numerical solution of the system 3 is plotted in Figure 7. Virus population is increasing whereas susceptible cell density decreases due to the infection. Without drug application, antibody response is low (Figure 7(d)), and thus infected cell or virus is increased.

Numerical solutions of the impulsive system for two different impulse intervals are plotted in Figure 8 for a fixed dosing rate. We can see that lower interval ($\tau = 1$ day) is capable of getting disease-free periodic orbit.

If we take higher interval of impulse ($\tau = 2$ days) with higher rate of dosing, then also we get the disease-free periodic orbit (Figure 9)

In Figure 10, we have observed the dynamics of antibody response for imperfect drug dosing corroborated with the subsection 4.1. To show the effects of taking drug holidays, we find the time from when a Covid-19 patient can take the required number of doses and then can miss the maximum number of doses. From this figure, we get the number of possible maximum drug holidays during the treatment period for a fixed drug dose and dosing interval. Taking the drug dose $\omega = 20$, dosing interval one day, the maximum number of the holiday is seven days, i.e., seven doses can be missed after fifty doses ($n - 1 = 50$). This figure also shows that after seven drug holidays,

 doi:10.20944/preprints202209.0090.v1

if the patient again takes 30 doses, then the antibody response will gain its previous equilibrium position ($n_2 = 30$).

6. Discussion and Conclusion

Worldwide human civilization has been struggling with COVID-19 since it seemed in Wuhan, China, in overdue 2019. Several nonpharmaceutical interventions like social distancing, wearing masks, sanitization, hand washing, quarantine, and lockdown have been initiated by the central government of each country guided by WHO. In spite of that, more than 30 million people are affected by COVID-19. Even though a number of vaccines like Covishield, covaxine, Pfizer, and sputnik are developed globally, and the vaccination campaign is going on, their effects are still a big question due to the mutation of the virus and new strain.

More attention is given to the target cell's limited modeling and the role of immune responses against the invaded SARS-CoV-2 virus in our respiratory system, which is the primary target area. In this study, we used the classical susceptible or uninfected cells, infected cells, and virus population in the presence of adaptive immune responses as a functional form. We computed the basic reproduction number R_0 for our model. We have observed that the model system has two equilibriums, one is disease-free ($\bar{P}$), and another is endemic equilibrium (P^*). The disease-free equilibrium is stable asymptotically when the basic reproduction number R_0 is below the unity. When theR_0 is greater than unity, the disease-free equilibrium becomes unstable and endemic equilibrium becomes feasible.

Here $R_0 = 1$ is the transcritical bifurcation point at which the system switches its stability from disease-free to endemic equilibrium. If the growth rate of the virus satisfies the relation $p > p^c = \frac{k\mu_1}{\beta\theta^2}$ at $R_0 = 1$, then the system moves into a bistability region, and this is called backward bifurcation. If $p < p^c$ at $R_0 = 1$ the system switches to forward bifurcation. This type of bifurcation at $R_0 = 1$ suggests a possibility of reinfection due to some external factors.

Finally, we have studied the effects of taking the drug in impulsive mode and also on holidays during the treatment. The optimum dosing interval is shown by numerical simulation that is $\tau = 1$ day for a fixed dose $\omega = 20$. This study also shows that for a short time treatment period, instead of taking the drug every one-day interval for the entire length of the induction period, it would be better if the patient takes seven days drug holiday after taking the first 50 doses.

In a nutshell, the proposed mathematical model successfully described the dynamics of Covid-19, and results from this study can further guide to development a cost-effective drug regimen for Covid-19 patients with fewer side effects.

Conflicts of Interest: The authors declare no conflict of interest.

1. Rossen, J.W.; Horzinek, M.C.; Rottler, P.J. Coronavirus infection of polarized epithelial cells. *Trends in microbiology* **1995**, *3*, 486–490.
2. Shahid Nadim, S.; Ghosh, I.; Chattopadhyay, J. Short-term predictions and prevention strategies for COVID-19: A model based study. *arXiv e-prints* **2020**, pp. arXiv–2003.
3. Volpert, V.; Banerjee, M.; Petrovskii, S. On a quarantine model of coronavirus infection and data analysis. *Mathematical Modelling of Natural Phenomena* **2020**, *15*, 24.
4. Okuonghae, D.; Omame, A. Analysis of a mathematical model for COVID-19 population dynamics in Lagos, Nigeria. *Chaos, Solitons & Fractals* **2020**, *139*, 110032.
5. Kucharski, A.J.; Russell, T.W.; Diamond, C.; Liu, Y.; Edmunds, J.; Funk, S.; Eggo, R.M.; Sun, F.; Jit, M.; Munday, J.D.; others. Early dynamics of transmission and control of COVID-19: a mathematical modelling study. *The lancet infectious diseases* **2020**, *20*, 553–558.
6. Shahzad, M.; Abdel-Aty, A.H.; Attia, R.A.; Khoshnaw, S.H.; Aldila, D.; Ali, M.; Sultan, F. Dynamics models for identifying the key transmission parameters of the COVID-19 disease. *Alexandria Engineering Journal* **2021**, *60*, 757–765.

7. Thomas, D.M.; Sturdivant, R.; Dhurandhar, N.V.; Debroy, S.; Clark, N. A primer on COVID-19 Mathematical Models. *Obesity* **2020**, *28*, 1375–1377.
8. Soukhovolsky, V.; Kovalev, A.; Pitt, A.; Kessel, B. A new modelling of the COVID 19 pandemic. *Chaos, Solitons & Fractals* **2020**, *139*, 110039.
9. Mondal, J.; Samui, P.; , A.N. Optimal control strategies of non-pharmaceutical and pharmaceutical interventions for COVID-19 control. *Journal of Interdisciplinary Mathematics* **2020**, pp. 1–29.
10. Chatterjee, A.N.; Basir, F.A.; Ahmad, B.; Alsaedi, A. A Fractional-Order Compartmental Model of Vaccination for COVID-19 with the Fear Factor. *Mathematics* **2022**, *10*, 1451.
11. Chatterjee, A.N.; Al Basir, F. A model for SARS-CoV-2 infection with treatment. *Computational and mathematical methods in medicine* **2020**, *2020*.
12. Nath, B.J.; Dehingia, K.; Mishra, V.N.; Chu, Y.M.; Sarmah, H.K. Mathematical analysis of a within-host model of SARS-CoV-2. *Advances in Difference Equations* **2021**, *2021*, 1–11.
13. Chatterjee, A.N.; Al Basir, F.; Almuqrin, M.A.; Mondal, J.; Khan, I. SARS-CoV-2 infection with lytic and non-lytic immune responses: A fractional order optimal control theoretical study. *Results in physics* **2021**, *26*, 104260.
14. Qureshi, S.; Yusuf, A. Fractional derivatives applied to MSEIR problems: Comparative study with real world data. *The European Physical Journal Plus* **2019**, *134*, 171.
15. Qureshi, S.; Yusuf, A.; Shaikh, A.A.; Inc, M. Transmission dynamics of varicella zoster virus modeled by classical and novel fractional operators using real statistical data. *Physica A: Statistical Mechanics and its Applications* **2019**, *534*, 122149.
16. Wang, S.; Pan, Y.; Wang, Q.; Miao, H.; Brown, A.N.; Rong, L. Modeling the viral dynamics of SARS-CoV-2 infection. *Mathematical biosciences* **2020**, *328*, 108438.
17. Nath, A.; Ahmad, B. A fractional-order differential equation model of COVID-19 infection of epithelial cells. *Chaos, Solitons & Fractals* **2021**, *147*, 110952.
18. Tang, S.; Ma, W.; Bai, P. A novel dynamic model describing the spread of the MERS-CoV and the expression of dipeptidyl peptidase 4. *Computational and mathematical methods in medicine* **2017**, *2017*.
19. Nath, A.; Al Basir, F. A model for sars-cov-2 infection with treatment. *Computational and mathematical methods in medicine* **2020**, *2020*.
20. Hernandez-Vargas, E.A.; Velasco-Hernandez, J.X. In-host mathematical modelling of covid-19 in humans. *Annual reviews in control* **2020**.
21. Carsetti, R.; Zaffina, S.; Piano Mortari, E.; Terreri, S.; Corrente, F.; Capponi, C.; Palomba, P.; Mirabella, M.; Cascioli, S.; Palange, P.; others. Different Innate and Adaptive Immune Responses to SARS-CoV-2 Infection of Asymptomatic, Mild, and Severe Cases. *Frontiers in immunology* **2020**, *11*, 3365.
22. Lu, X.; Xiang, Y.; Du, H.; Wing-Kin Wong, G. SARS-CoV-2 infection in children–Understanding the immune responses and controlling the pandemic. *Pediatric Allergy and Immunology* **2020**, *31*, 449–453.
23. Zhou, Z.; Ren, L.; Zhang, L.; Zhong, J.; Xiao, Y.; Jia, Z.; Guo, L.; Yang, J.; Wang, C.; Jiang, S.; others. Heightened innate immune responses in the respiratory tract of COVID-19 patients. *Cell host & microbe* **2020**, *27*, 883–890.
24. Shayakhmetov, D.M. Virus infection recognition and early innate responses to non-enveloped viral vectors. *Viruses* **2010**, *2*, 244–261.
25. Biswas, D.; Roy, P.K.; Li, X.Z.; Basir, F.A.; Pal, J. Role of macrophage in the disease dynamics of cutaneous Leishmaniasis: a delay induced mathematical study. *Commun. Math. Biol. Neurosci.* **2016**, *2016*, Article–ID.
26. Spangelo, B.L.; Gorospe, W.C. Role of the cytokines in the neuroendocrine-immune system axis. *Frontiers in neuroendocrinology* **1995**, *16*, 1–22.
27. Roy, A.K.; Al Basir, F.; Roy, P.K. A vivid cytokines interaction model on psoriasis with the effect of impulse biologic (TNF- α inhibitor) therapy. *Journal of Theoretical Biology* **2019**, *474*, 63–77.
28. Du, S.Q.; Yuan, W. Mathematical modeling of interaction between innate and adaptive immune responses in COVID-19 and implications for viral pathogenesis. *Journal of medical virology* **2020**, *92*, 1615–1628.
29. Van den Driessche, P.; Watmough, J. Reproduction numbers and sub-threshold endemic equilibria for compartmental models of disease transmission. *Mathematical biosciences* **2002**, *180*, 29–48.

30. Lou, J.; Smith, R.J. Modelling the effects of adherence to the HIV fusion inhibitor enfuvirtide. *Journal of theoretical biology* **2011**, *268*, 1–13.
31. Roy, P.K.; , A.N.; Li, X.Z. The effect of vaccination to dendritic cell and immune cell interaction in HIV disease progression. *International Journal of Biomathematics* **2016**, *9*, 1650005.
32. Castillo-Chavez, C.; Song, B. Dynamical models of tuberculosis and their applications. *Mathematical Biosciences & Engineering* **2004**, *1*, 361.
33. Yu, H.; Zhong, S.; Agarwal, R.P. Mathematics analysis and chaos in an ecological model with an impulsive control strategy. *Communications in Nonlinear Science and Numerical Simulation* **2011**, *16*, 776–786.
34. Lakshmikantham, V.; Simeonov, P.S.; others. *Theory of impulsive differential equations*; Vol. 6, World scientific, 1989.
35. Miron, R.; Smith, R. Modelling imperfect adherence to HIV induction therapy. *BMC infectious diseases* **2010**, *10(1)*, p.6.
36. Wölfel, R.; Corman, V.M.; Guggemos, W.; Seilmaier, M.; Zange, S.; Müller, M.A.; Niemeyer, D.; Jones, T.C.; Vollmar, P.; Rothe, C.; others. Virological assessment of hospitalized patients with COVID-2019. *Nature* **2020**, *581*, 465–469.
37. Hethcote, H.W. The mathematics of infectious diseases. *SIAM review* **2000**, *42*, 599–653.
38. Osuna, O.; Villaseñor, G. On the Dulac functions. *Qualitative Theory of Dynamical Systems* **2011**, *10*, 43–49.

Appendix G

Proof of theorem 5 is given below:

Proof. In the absence of SARS-CoV-2, the uninfected epithelial cell E_S satisfy the equation

$$\frac{dE_S(t)}{dt} = \Pi - \mu_1 E_S(t). \tag{A47}$$

The solution of the equation (A47) is

$$E_S(t) = \frac{\Pi}{\mu_1} - \Big(\frac{\Pi}{\mu_1} - E_S(0)\Big)e^{-\mu_1 t}. \tag{A48}$$

It follows that $E_S(t) \to \frac{\Pi}{\mu_1}$ when $t \to \infty$. If the initial value satisfy $E_S(0) < \frac{\Pi}{\mu_1}$ then all the trajectories remain below $\frac{\Pi}{\mu_1}$. Also if the initial vale satisfy $E_S(0) > \frac{\Pi}{\mu_1}$ then all the trajectories remain above $\frac{\Pi}{\mu_1}$. □

Let us assume $E_S(t) \leq \frac{\Pi}{\mu_1}$ i.e., initial values are at or below its steady state and this can be proved in our globally asymptotically stability at disease free equilibrium $\bar{P}$.

We assume a Liapunov function in following form

$$\mathcal{L}_{\mathcal{E}}(t) = \mathcal{A}E_I(t) + \mathcal{B}V(t), \tag{A49}$$

where $\mathcal{A}$ and $\mathcal{B}$ both are positive.

Then the derivative of Liapunov function

$$\begin{aligned}
\frac{d\mathcal{L}_{\mathcal{E}}(t)}{dt} &= \mathcal{A}\frac{dE_I(t)}{dt} + \mathcal{B}\frac{dV(t)}{dt}, \\
&= \mathcal{A}(\beta E_S V - \mu_2 E_I) + \mathcal{B}\{pE_I - \big(\mu_3 + \frac{kE_I}{V+\theta}\big)V\}, \\
&\leq (\mathcal{A}\frac{\beta\Pi}{\mu_1} - \mathcal{B}\mu_3)V + (\mathcal{B}p - \mathcal{A}\mu_2)E_I.
\end{aligned} \tag{A50}$$

Preprints (www.preprints.org) | NOT PEER-REVIEWED | Posted: 6 September 2022 doi:10.20944/preprints202209.0090.v1

Let $\mathcal{A} = 1,\ \mathcal{B} = \frac{\beta\Pi}{\mu_1\mu_2}$, then

$$\begin{aligned} \frac{d\mathcal{L}_{\mathcal{E}}(t)}{dt} &\leq (\frac{p\beta\Pi}{\mu_1\mu_3} - \mu_2)E_I, \\ &\leq \frac{p\beta\Pi}{\mu_1\mu_2\mu_3}(R_0 - 1)E_I. \end{aligned} \tag{A51}$$

Then we have $\frac{d\mathcal{L}_{\mathcal{E}}}{dt} \leq 0$ when $R_0 \leq 1$ and $\frac{d\mathcal{L}_{\mathcal{E}}}{dt} = 0$ implies $E_I = 0$ when $t \to \infty$. Then disease free equilibrium is globally asymptotically stable when $R_0 \leq 1$ by the Liapunov Lasalle's Theorem [37]. This completes the proof.

Appendix H

Proof of theorem 8 is given below:

Proof. Let us assume the existence of endemic equilibrium point P^* and the following function is defined in R^3_+. We now consider the Dulac function in the following form [38]:

$$\mathcal{D} = \frac{1}{E_S E_I}, \tag{A52}$$

and we use (25) for the endemic equilibrium point P^*. Then

$$\frac{\partial(\mathcal{D}f_1)}{\partial E_S} = -\frac{\Pi}{E_S^2 E_I} < 0,$$

$$\frac{\partial(\mathcal{D}f_2)}{\partial E_I} = -\frac{\beta V}{E_I^2} < 0, \tag{A53}$$

$$\frac{\partial(\mathcal{D}f_3)}{\partial V} = -\frac{1}{E_S E_I}\left(\mu_3 + \frac{k\theta E_I}{(V+\theta)^2}\right) < 0. \tag{A54}$$

Then

$$\frac{\partial(\mathcal{D}f_1)}{\partial E_S} + \frac{\partial(\mathcal{D}f_2)}{\partial E_I} + \frac{\partial(\mathcal{D}f_3)}{\partial V} = -\frac{\Pi}{E_S^2 E_I} - \frac{\beta V}{E_I^2} - \frac{1}{E_S E_I}\left(\mu_3 + \frac{k\theta E_I}{(V+\theta)^2}\right), \tag{A55}$$

which is clearly negative. Thus all solution of system (4) tends to one equilibrium point globally. □